Supporting Information for "Along-strike segmentation of seismic tremor and its relationship with the hydraulic structure of the subduction fault zone"

Gaspard Farge[1*], Claude Jaupart[1] and Nikolai M. Shapiro[2]

[1]Université de Paris, Institut de Physique du Globe de Paris, CNRS, F-75005 Paris, France

[2]Institut de Sciences de la Terre, Université Grenoble Alpes, CNRS (UMR5275), Grenoble, France

Contents of this file

S1. Tremor patterns in two other subduction zones

In subductions where the extent of observations along strike is wide enough, the observed tremor activity is segmented along strike, varying both in temporal clustering, timescale and regularity of burst recurrence. Here, we show two additional examples of this segmentation along-strike in the Central American subduction zone (Figure S1), and in the Cascadia subduction zone.

S2. Characterizing clustering intensity and recurrence timescales

S2.1. Point process description

We introduce elements of the point process formalism that will be used to formally describe the analysis of tremor intermittence. In the point process formalism, an event catalog — earthquakes, LFEs, valve openings — can be represented by the function $N_{ev}(t)$, a monotonically increasing function of time t, that increases in steps of 1, when the time is equal to an event time $t = t_i$. The point process can be formally written as $\mathrm{d}N_{ev}(t)$, a spike of one each time $t = t_i$. However, a more practical and as complete description of the process is to use the series of event times:

$$\{t_i\} \text{ for } 1 \leq i \leq N_{ev}^{tot}, \tag{1}$$

where N_{ev}^{tot} is the total number of events considered in the analyzed subset. One can also work with the *inter-event times* Δt_i, defined as the time since the previous event

$$\{\Delta t_i\} = t_i - t_{i-1} \text{ for } i > 1. \tag{2}$$

The *event count time series* $C_j(\delta t)$, or *sequence of counts*, is another representation of the point process. It counts the number of events in successive and contiguous bins of duration δt, between time $t = j\delta t$ and $t = (j + 1)\delta t$:

$$C_j(\delta t) = N_{ev}[(j + 1)\delta t] - N_{ev}[j\delta t] \tag{3}$$

S2.2. Characterizing clustering intensity

The objective of this analysis is to quantify the extent to which events occur within clusters, rather than as a more homogeneous process in time. We detect clusters as peaks in the event count time series (see equation 3): a count of the number of events in bins of length δt. In our parametrization, peaks of activity are defined as all consecutive bins in which the event count is higher than a given threshold. In order to select more intense periods of activity, peaks are defined as periods during which activity is more intense than 66% of the time, and should therefore cover 34% of the analyzed period (Figure S3): the 34% most active δt-bins. We can define the peak cover f_{peaks} as the fraction of the time covered by peaks, compared to the total time of the analyzed period. Because of the discrete nature of the event counting process, the fraction of the time that is covered by peaks f_{peaks} is never exactly 34% of the time:

$$f_{peaks} = T^{peaks}/T^{tot} \approx 0.34 \tag{4}$$

where T^{peaks} is the cumulative duration of peaks in the time series, and T^{tot} the total duration of the time series.

Although peaks always cover about a third of the studied period, in a clustered time series, most events — more than a third — will occur during peaks, that is 34 % of the time. To discriminate between a clustered and not clustered activity, we will therefore work with the proportion of events that occur within peaks, p_{ev}^{peaks}. When the activity can be described as a Poisson point process, or if the event count is normally distributed around an average value, the events are as much in "peaks" that in the "background", as defined by the 34%-threshold (Figure S3c, d, e and f). The number of events in peaks N_{ev}^{peaks} should therefore sum to about a third of events, as peaks are defined by the upper tritile of event counts. On the other hand, if the events cluster in time, events should concentrate in peaks. Peaks still cover about 34% of the time series, but most event (at least more than 34% of them) occur in peaks (*e.g* Figure S3a and b). A simple measure of clustering can therefore be constructed by mapping linearly the proportion of events in peaks p_{ev}^{peaks} to 0 – 1. We thus define the *clustering index* c: if 100% of events are in peaks, events occur only in clusters and $c = 1$, if only 34% of events occur in peaks, events are more or less as likely to occur in peaks as outside of peaks, the activity is not clustered and $c = 0$.

$$c = \frac{p_{ev}^{peaks} - f_{peaks}}{1 - f_{peaks}} \tag{5}$$

where f_{peaks} is the fraction of the studied period that is covered with peaks, that is always approximately $f_{peaks} \approx 0.34$. In Figure S3, three cases show values of the clustering index c for two simulations (highly and not temporally clustered) and a Poisson process. We use the clustering index c as a measure of clustering intensity in observed LFE catalogs (Figure 1) and in simulated event catalogs (Section 5, Figures 9 and 11).

S2.3. Measuring recurrence timescales

In both real cases (Figure 1, main text) and simulations (Figure 9), clusters of seismic events can sometimes exhibit identifiable, characteristic timescales of recurrence. Our aim is to quantify the longest recurrence timescales

present in the activity, and estimate how variable they are throughout the studied period. To do so, we design an automated analysis that explicitly identifies clusters of events based only on the proximity of their occurrence time t_i, classifies clusters based on the number of events they are made of, and finally measures the recurrence of clusters of a same class of size. We perform this analysis only in cases when the activity is clustered: when more than 50% of events occur in peaks ($c > 0.25$) — peaks are defined as the 34% most active periods of the studied period. Figure S3c to f show two examples of simulations that exhibit no clustering of activity, on which no timescale analysis is therefore performed.

The first step of the recurrence analysis is to identify clusters of events, based on their proximity in time. In order to de-noise the event time time-series, we start by removing all events outside of the peaks detected in the temporal clustering analysis. We then regroup the remaining events into clusters, by performing a density-based clustering algorithm (DBSCAN, (Ester et al., 1996), *scikit-learn* implementation (Pedregosa et al., 2011)) on their occurrence times t_i. The clustering algorithm labels events as isolated or belonging to a cluster based on two parameters: the neighborhood radius (a delay in time, in our case) ϵ and the minimum number of events N_{min} that have to be at a delay of ϵ from one another so that they are considered in the same cluster. Those two parameters therefore provide an estimation of the minimum density of events needed around an event for it to be in a cluster. By iterating from event to event in a dense neighborhood, the algorithm identifies which events are within clusters, and which are isolated. We choose $\epsilon = \max_i(\Delta t_i)/4$, a fourth of the maximum inter-event delay measured in the de-noised event times. We empirically verify that this value allows to automatically detect the largest clusters, without splitting them when the activity rate is temporarily low within them. And for the minimum number of events, we choose $N_{min} = 10$ for simulated seismicity ($N_{min} = 300$ for the Shikoku case, in Figure 1), based on the total number of events in each case. At the end of this step, all events are affiliated to a cluster (labelled) k, or identified as isolated (noise). In order to avoid windowing artifacts, we discard the events of the first and last identified clusters as noise. Figure S4a and b depict this first step of the recurrence analysis.

In some cases, the detected clusters can be grouped into identifiable classes of size, and in each class, the clusters recur with a specific delay. In this second step, our objective is therefore to group event clusters based on their sizes S_k, defined as the number of events that belong to it. As cluster sizes sometimes span orders of magnitudes, we perform the DBSCAN clustering algorithm on the logarithm base 10 of cluster sizes. For the DBSCAN parameters, we choose the neighborhood distance $\epsilon = 0.15 * \log_{10}(S_{max}/S_{min})$ where S_{max} and S_{min} are the maximum and minimum cluster sizes in the analyzed case, and $N_{min} = 2$. Those parameters successfully group clusters into classes of different characteristic sizes, while allowing for variability in size within a given class of clusters. At the end of this step, all clusters are labelled as belonging to one or several classes, based on their size. It is more common that one size of cluster only is identified, but in some cases, two (Figure S4) or more rarely three classes can be identified with certainty. In the example simulation shown in Figure S4b and c, the algorithm detected a class of large clusters (in hot colors) and a class of small clusters (in cold colors).

The final step is to measure the recurrence delay between clusters. Within a class of clusters, we measure the delays ΔT_k between the centroids T_k of contiguous clusters (defined as the average event occurrence time within that cluster). As it appears that both in simulations and real cases the smaller clusters occur more frequently than, and therefore in between, larger clusters, contiguous clusters are considered to be clusters of the same size with no larger clusters occurring in between. In practice, the delays between two clusters is measured only when there are no larger cluster in between (see Figure S4c). The average delay $\text{mean}_k(\Delta T_k)$ between clusters of a class gives an estimation of the recurrence timescale for this class, and the standard deviation $\text{std}_k(\Delta T_k)$ allows to estimate how variable it is. The ratio of the standard deviation to the average recurrence timescale $\text{std}_k(\Delta T_k)/\text{mean}_k(\Delta T_k)$, called the coefficient of variation, gives an estimation of how regular the recurrence is, or how periodic it is.

Figures S5 and S6 provide additional examples of the clustering and recurrence analysis for the highly clustered, loosely periodic activity of segment 6 of the Shikoku tremor zone (Poiata et al., 2021) and finally an intermediate case, where the simulated seismicity is weakly clustered, and the recurrence is measured with a strong variability.

S3. Full valve-distribution space

In the next two Figures (Figure S7 and S8), we show one example of a valve distribution for all $(u, \overline{d_v})$ parameters of the Weibull distribution used to design valve systems in Section 5. For the parameter space exploration there, 30 distributions were drawn for each $(u, \overline{d_v})$ couple.

References

Brudzinski, M. R., & Allen, R. M. (2007). Segmentation in episodic tremor and slip all along Cascadia. *Geology*, *35*(10), 907. doi: 10.1130/G23740A.1

Brudzinski, M. R., Hinojosa-Prieto, H. R., Schlanser, K. M., Cabral-Cano, E., Arciniega-Ceballos, A., Diaz-Molina, O., & DeMets, C. (2010, August). Nonvolcanic tremor along the Oaxaca segment of the Middle America subduction zone. *Journal of Geophysical Research*, *115*, B00A23. doi: 10.1029/2008JB006061

Ester, M., Kriegel, H.-P., Sander, J., & Xu, X. (1996). A Density-Based Algorithm for Discovering Clusters in Large Spatial Databases with Noise. *Proceedings of the 2nd International Conference on Knowledge Discovery and Data mining*, 226–231.

Frank, W. B., Shapiro, N. M., Husker, A. L., Kostoglodov, V., Romanenko, A., & Campillo, M. (2014, October). Using systematically characterized low-frequency earthquakes as a fault probe in Guerrero, Mexico. *Journal of Geophysical Research: Solid Earth*, *119*(10), 7686–7700. doi: 10.1002/2014JB011457

Hayes, G. (2018). *Slab2 - A Comprehensive Subduction Zone Geometry Model.* U.S. Geological Survey. doi: 10.5066/F7PV6JNV

Husker, A., Frank, W. B., Gonzalez, G., Avila, L., Kostoglodov, V., & Kazachkina, E. (2019, January). Characteristic Tectonic Tremor Activity Observed Over Multiple Slow Slip Cycles in the Mexican Subduction Zone. *Journal of Geophysical Research: Solid Earth*, *124*(1), 599–608. doi: 10.1029/2018JB016517

Pedregosa, F., Varoquaux, G., Gramfort, A., Michel, V., Thirion, B., Grisel, O., ... Duchesnay, É. (2011). Scikit-learn: Machine Learning in Python. *Journal of Machine Learning Research*, *12*(85), 2825–2830.

Poiata, N., Vilotte, J.-P., Shapiro, N. M., Supino, M., & Obara, K. (2021, November). Complexity of Deep Low-Frequency Earthquake Activity in Shikoku (Japan) Imaged From the Analysis of Continuous Seismic Data. *Journal of Geophysical Research: Solid Earth*, *126*(11). doi: 10.1029/2021JB022138

Wech, A. G. (2010, July). Interactive Tremor Monitoring. *Seismological Research Letters*, *81*(4), 664–669. doi: 10.1785/gssrl.81.4.664

Wech, A. G., & Creager, K. C. (2008, October). Automated detection and location of Cascadia tremor. *Geophysical Research Letters*, *35*(20), L20302. doi: 10.1029/2008GL035458

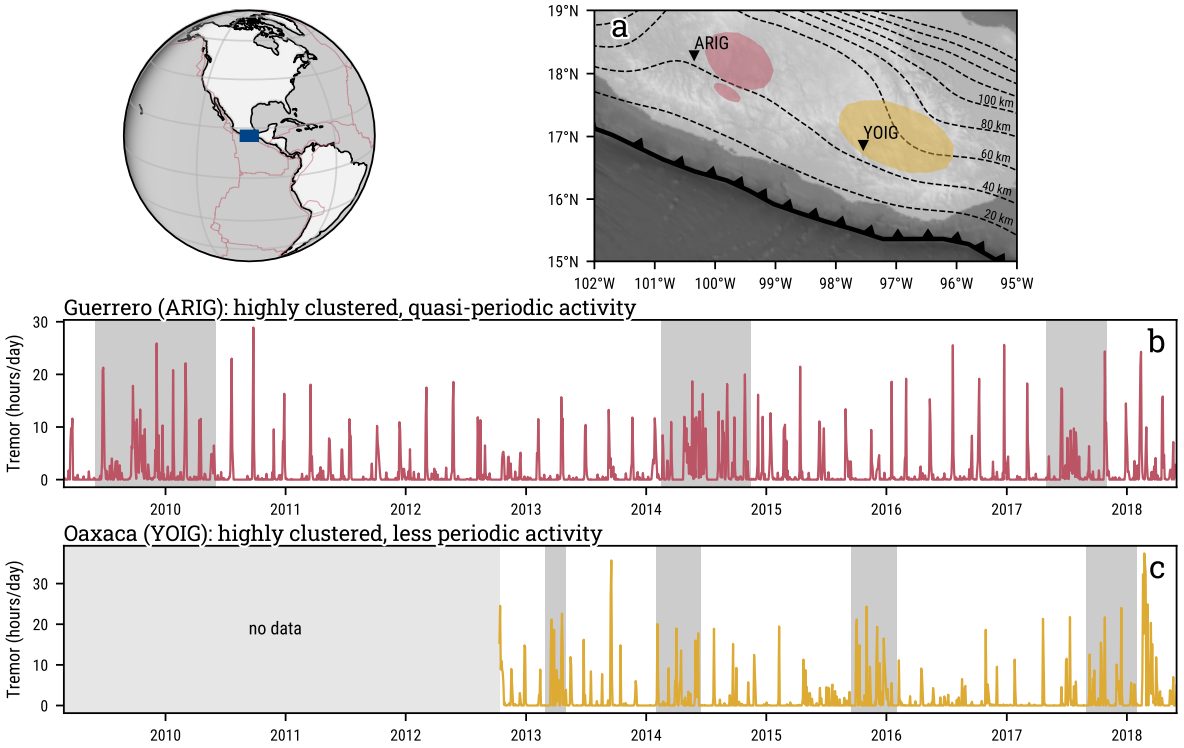

Figure S1: Segmentation of tremor intermittence in Mexico (Central American subduction zone, 2009–2018). *(a)* Map of tremor activity in the subduction zone. Colored patches outline the extent of the source regions (Brudzinski et al., 2010; Frank et al., 2014). The stations used to detect daily tremor activity are shown with black triangles. Depth contours of the slab are taken from Slab2 (Hayes, 2018). The thick black line outlines the trench. Tremor activity rate is measured in hours of tremor per day in *(b)* Guerrero, measured at station ARIG, and *(c)* Oaxaca, measured at station YOIG. Tremor data from Husker et al. (2019). On both *(b)* and *(c)* the periods shaded in dark grey represent geodetically detected slow slip events (Husker et al., 2019). The two zones show different intermittence patterns. In Guerrero, large bursts of tremor occur quasi-periodically every 2–3 months, in between the intense tremor episodes occurring with SSEs every 3.5 years. In Oaxaca, inter-SSE bursts are less periodic, recurring every 1–3 months, in between longer tremor episodes associated with large SSEs, roughly every 2.5 years.

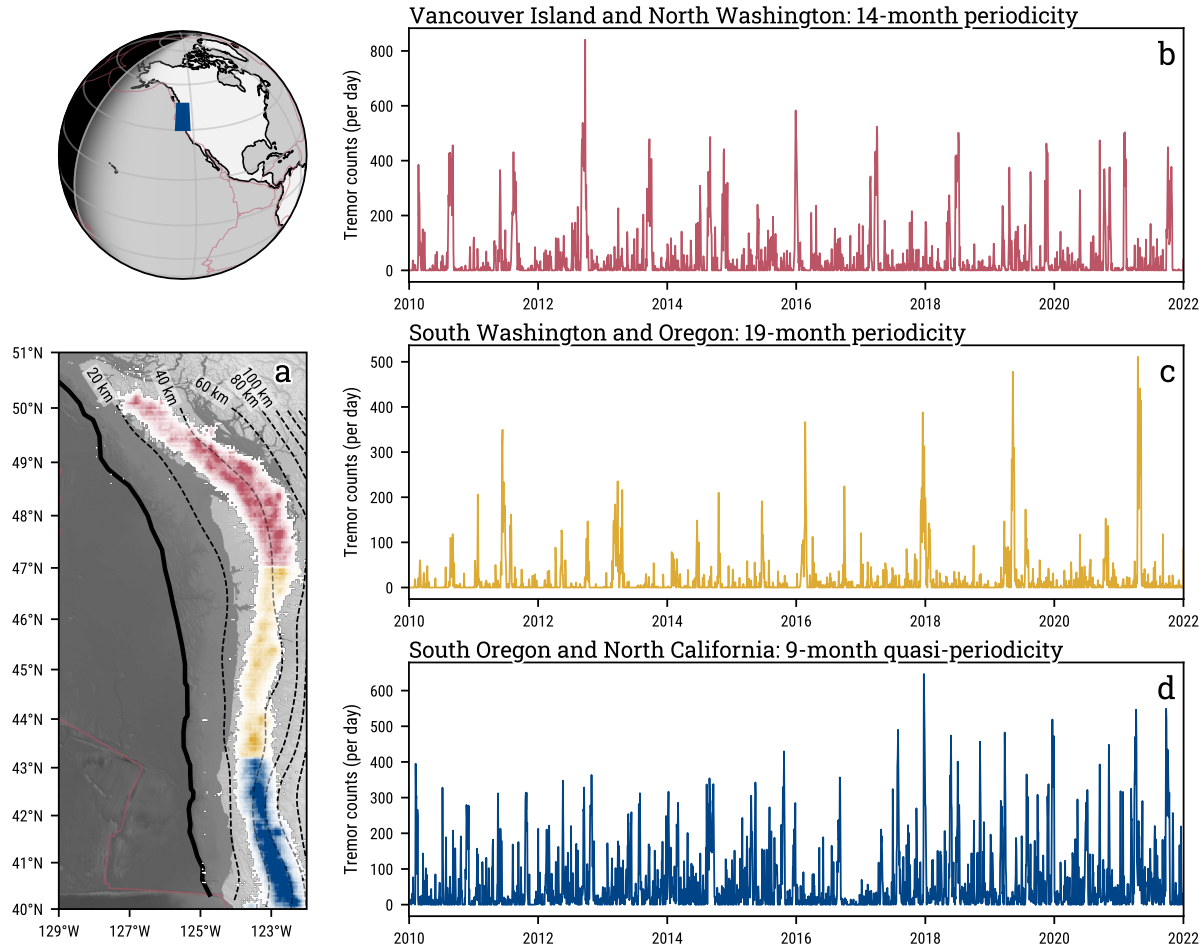

Figure S2: Segmentation of tremor intermittence in Cascadia (2010–2022). *(a)* Map of tremor activity in the subduction zone, colored according to source density and segmentation (as defined by Brudzinski and Allen (2007)), tremor epicenter catalog from Wech and Creager (2008); Wech (2010). Depth contours of the slab are taken from Slab2 (Hayes, 2018). The thick black line outlines the trench. Tremor activity rate in epicenter counts per day under *(b)* Vancouver Island and Northern Washington, *(c)* South Washington and Oregon, *(d)* South Oregon and Northern California. The periodicity estimates are from Brudzinski and Allen (2007). The activity is segmented along strike: the northernmost segment is most periodic, the center segment is less periodic, with a longer timescale of recurrence and higher level of clustering, and the southernmost segment is least clustered, with a shorter recurrence scale of tremor bursts.

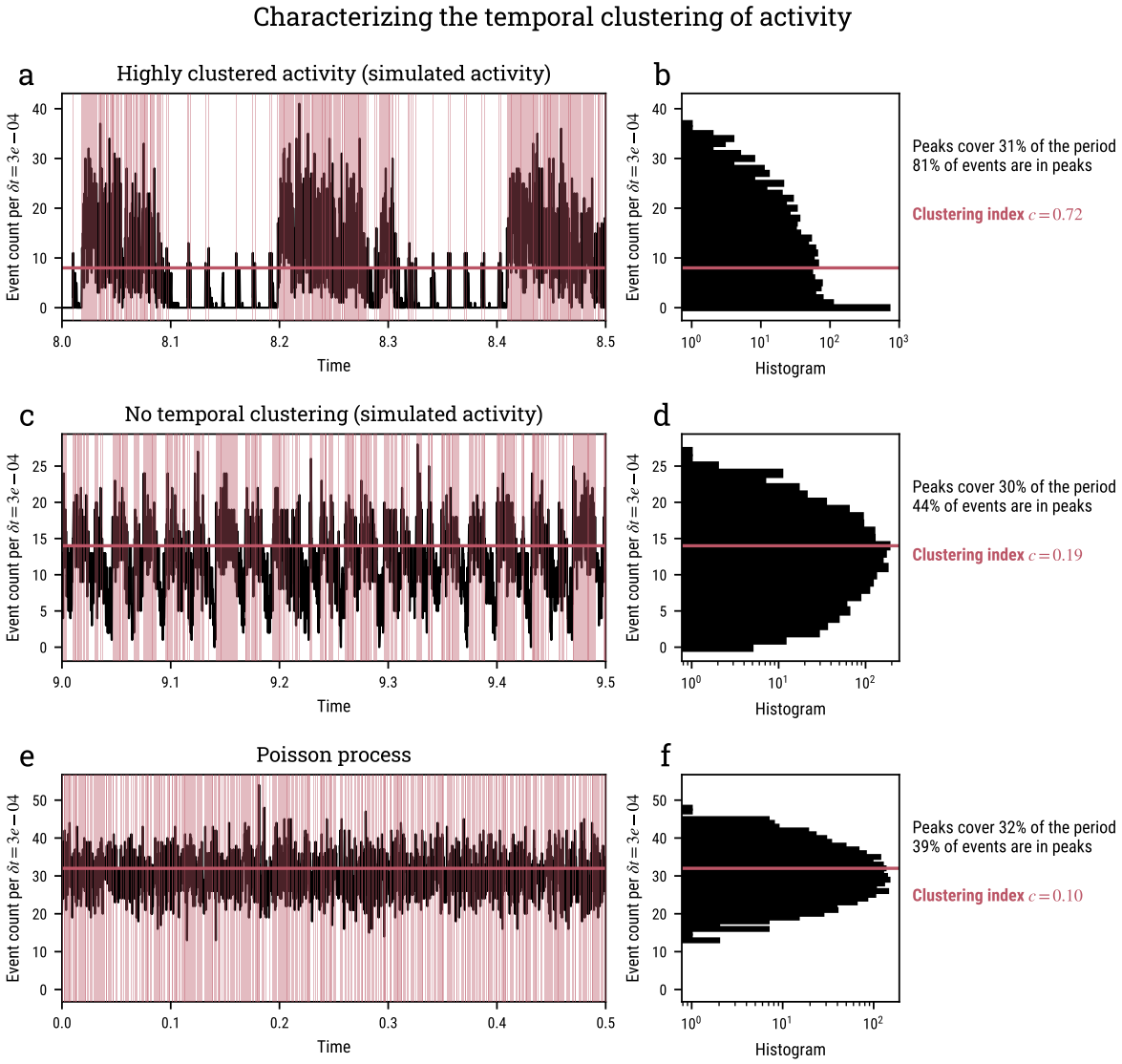

Figure S3: Clustering analysis of *(a)*, *(b)* a simulated, highly clustered activity in a clustered valve system with $N_v = 43$ valves ($\overline{d_v} = 1w_v$), $u = 0.3$, under a input flux of $q_{in} = 0.16$, *(b)*, *(c)* a simulated activity without temporal clustering, in a Poissonian valve system with $N_v = 29$ valves ($\overline{d_v} = 2w_v$), $u = 1.0$, under a input flux of $q_{in} = 0.16$, and *(e)*, *(f)* a Poisson process, with event rate $r = 30$ events per $\delta t = 3 \times 10^{-4}$ scaled time units. In *(a)*, *(c)*, and *(e)*, the event count time series are represented in black with the threshold defining peaks as the red horizontal line, corresponding to the 66% quantile of the event count distribution, represented in *(b)*, *(d)* and *(f)*. The fraction of time that peaks represent f_{peaks}, the proportion of events within peaks p_{ev}^{peaks} and clustering index c for each case are listed on the right.

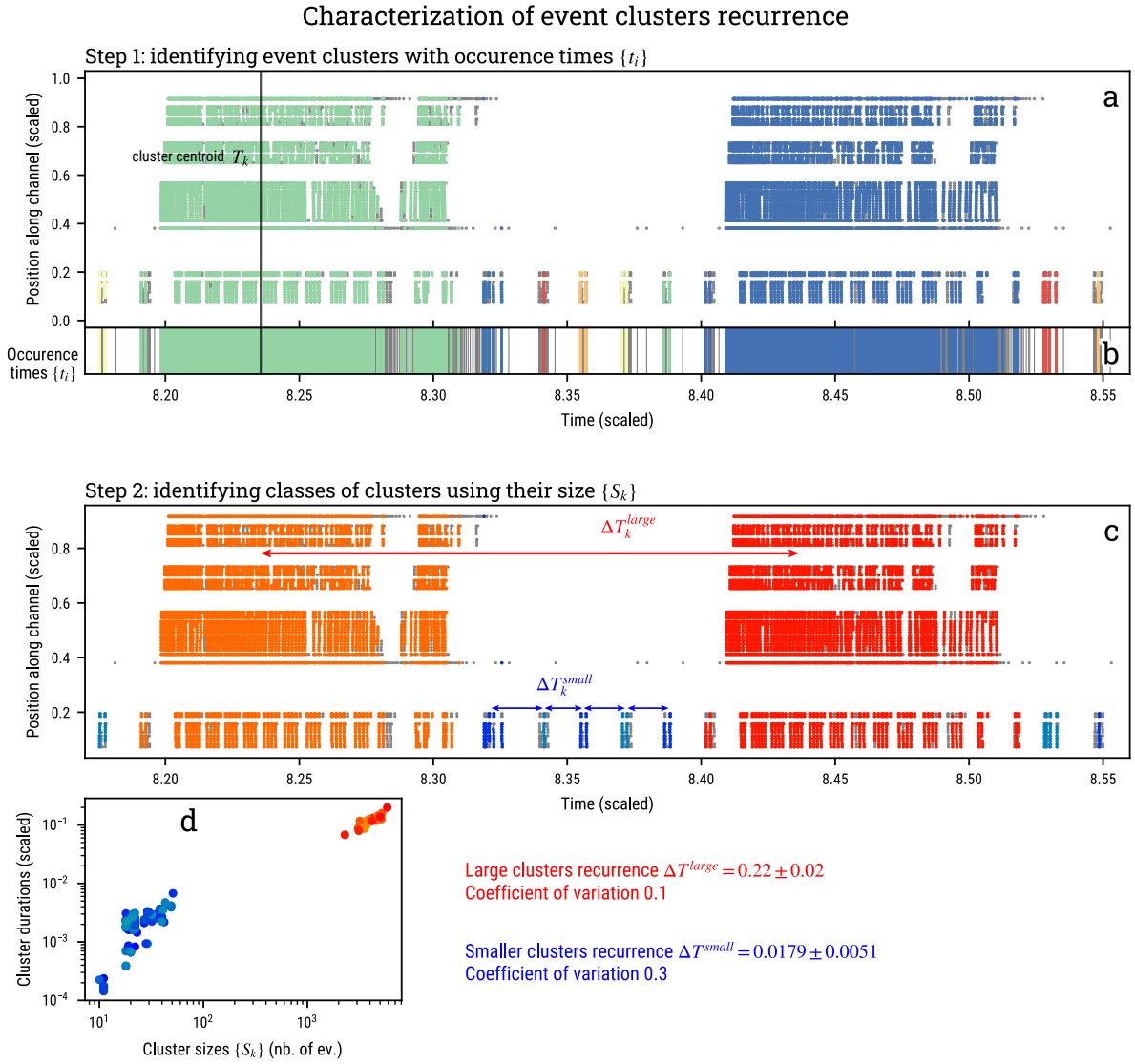

Figure S4: Recurrence analysis of a simulated, highly clustered activity in a clustered valve system with $N_v = 43$ valves ($\overline{d_v} = 1 w_v$), $u = 0.3$, under a input flux of $q_{in} = 0.16$ (activity count in Figure S3a). In a first step, the algorithm detects clusters of events using the occurrence times. *(a)* Time-dip representation of activity, each point corresponds to an events. Events are colored according to which cluster they are labelled into. The grey dots are labelled as noise, either in the de-noising step, or by the clustering algorithm. The clustering algorithm is performed only on occurrence times, represented as horizontal lines in *(b)*, with the same color-coding as in *(a)*. The centroid of each cluster T_k is computed as the average occurrence time of events that belong to each one of them. In a second step, clusters of events are grouped into classes, based on their sizes. Two sizes of clusters are detected for this simulation, small clusters in blue shades, and large clusters in orange to red shades. *(c)* Time-dip representation of events, with events colored according to the cluster and class they belong to. The delays ΔT_k between cluster centroids of each class are indicated with arrows. *(d)* The size-duration distribution of clusters of events. The classifying step only considers the size of clusters.

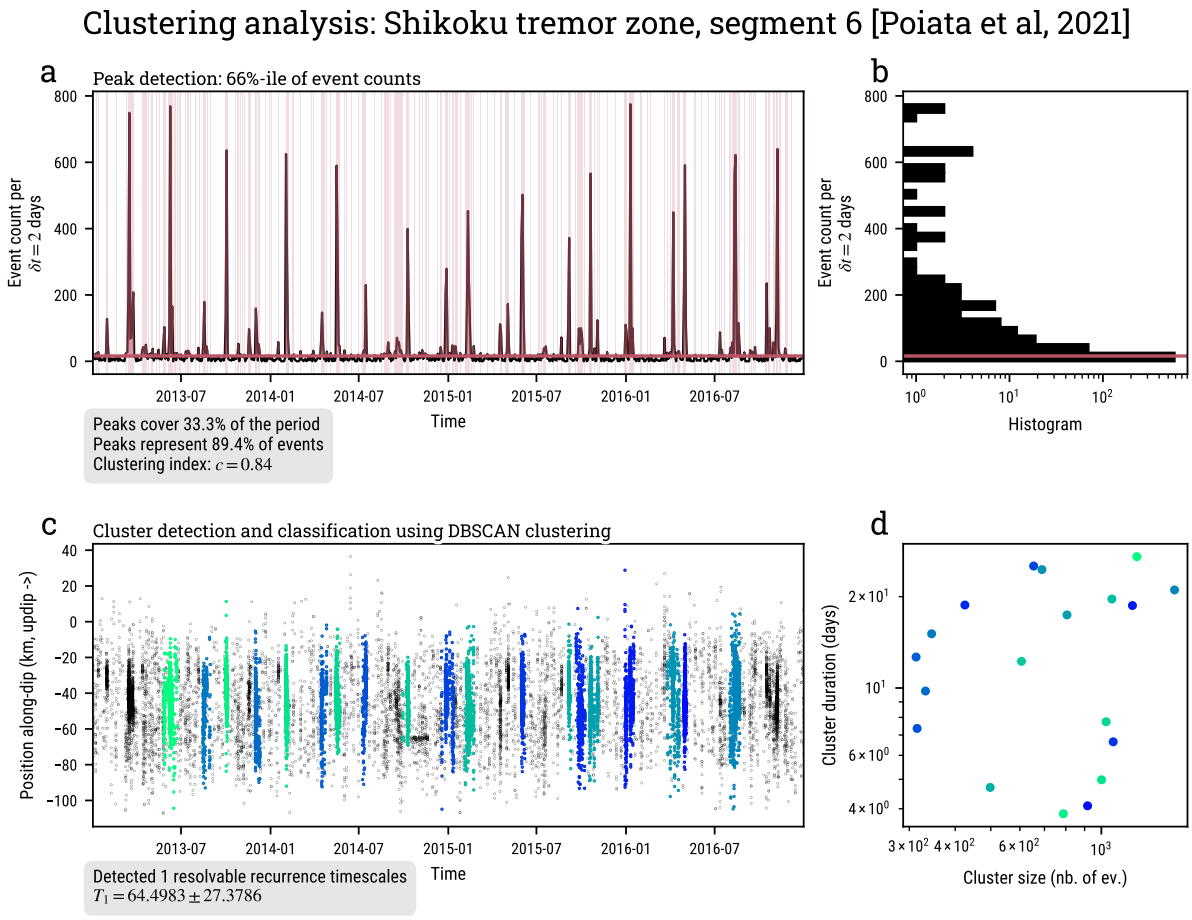

Figure S5: Clustering analysis of LFEs in the segment 6 poiata2021Complexity of the Shikoku tremor zone. *(a)* Event count time series. The threshold defining peaks is represented as the horizontal red line, and corresponds to the 66% quantile of the event count distribution, represented in *(b)*. The short intervals colored in light red in *(a)* are the peaks, as defined previously. *(c)* shows the activity in time and space, projected along the dip of the fault. Colors show how events are labelled into clusters. *(d)* shows the duration and size distribution of clusters identified for the full simulation. Only one type of cluster is identified by the algorithm in this case.

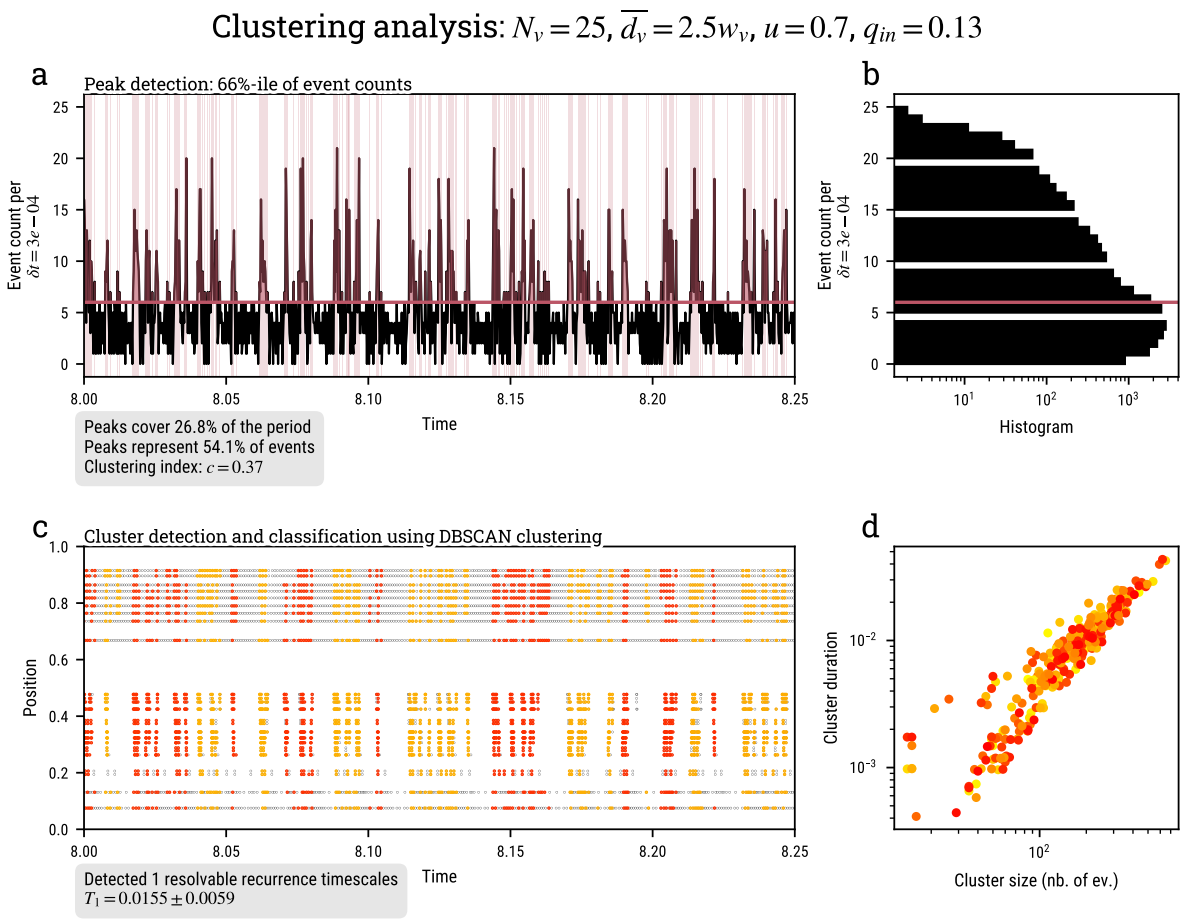

Figure S6: Clustering analysis of a simulated, weakly clustered activity in a clustered valve system with $N_v = 25$ valves ($\overline{d_v} = 2.5w_v$), $u = 0.7$, under a input flux of $q_{in} = 0.13$. *(a)* Event count time series. The threshold defining peaks is represented as the horizontal red line, and corresponds to the 66% quantile of the event count distribution, represented in *(b)*. The short intervals colored in light red in *(a)* are the peaks, as defined previously. *(c)* shows the activity in time and along the channel, colors show how events are labelled into clusters. *(d)* shows the duration and size distribution of clusters identified for the full simulation. In this case, only one class of clusters is identified by the algorithm, with a high variability of sizes and durations.

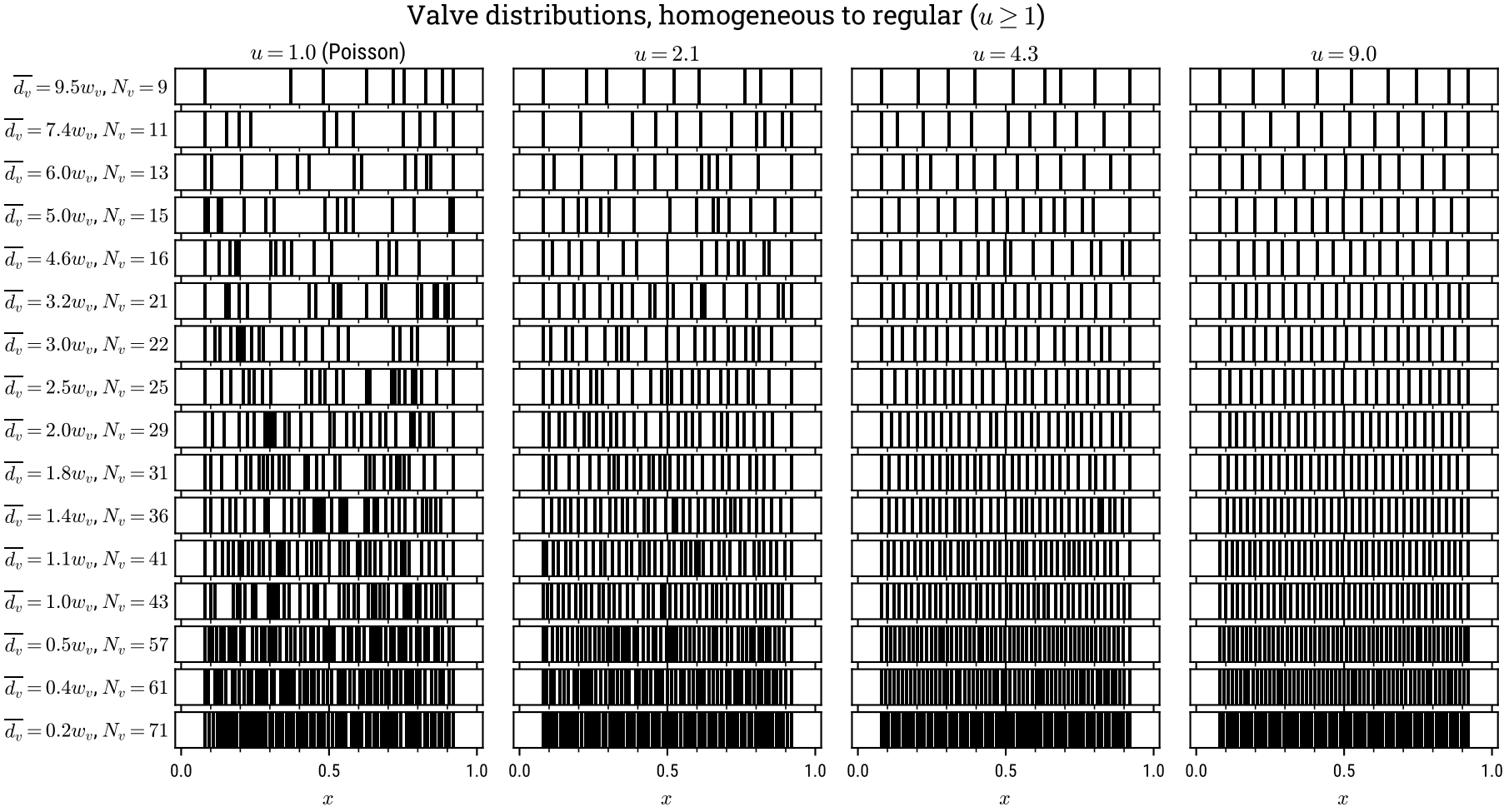

Figure S7: An example of valve distribution drawn from every $(u, \overline{d_v})$ explored in the simulations, here for Poissonian to regular valve distributions.

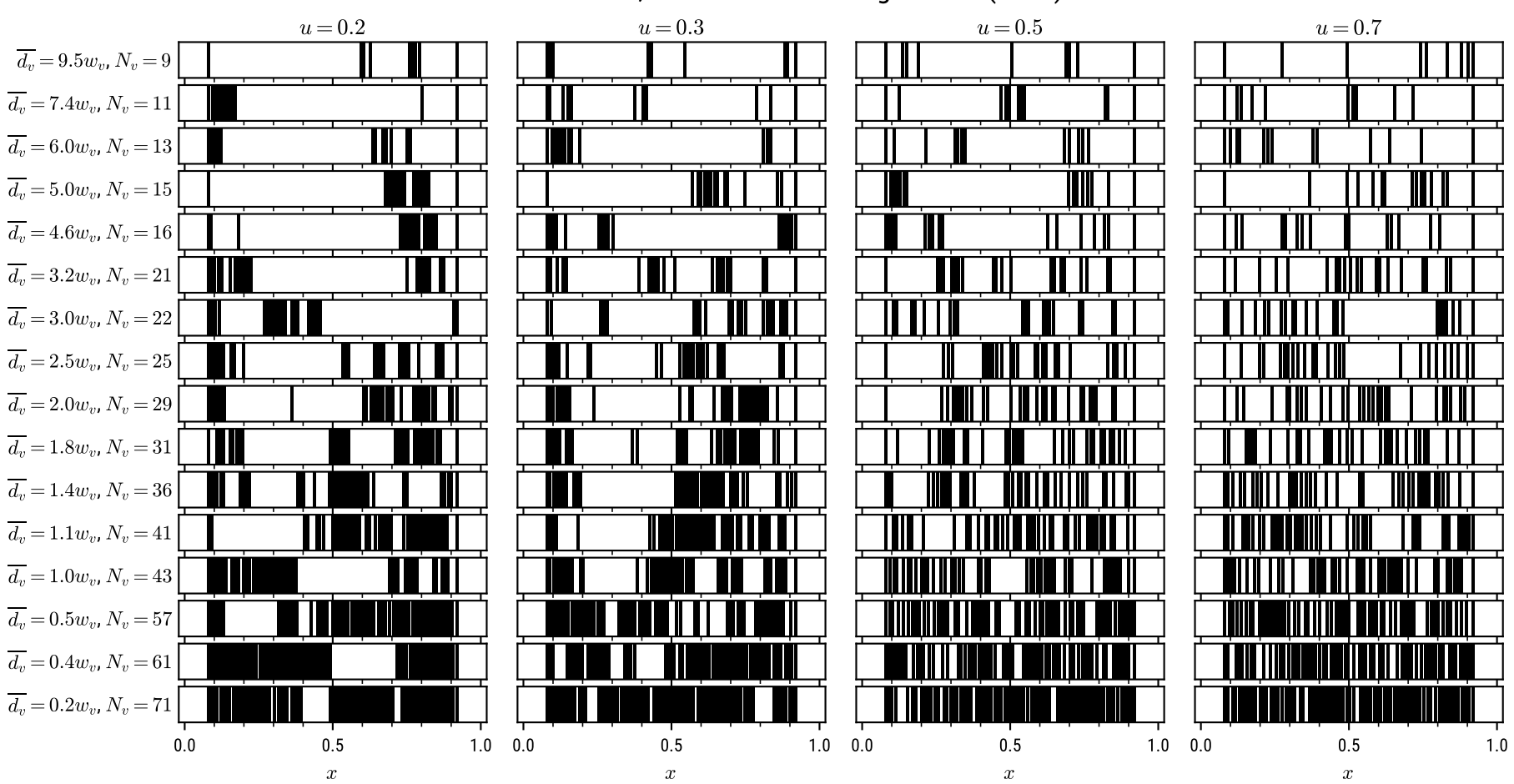

Figure S8: An example of valve distribution drawn from every $(u, \overline{d_v})$ explored in the simulations, here for clustered to Poissonian valve distributions.